Ultra-Wideband Impedance Spectroscopy of a Live Biological Cell

Xiao Ma[©], Student Member, IEEE, Xiaotian Du, Graduate Student Member, IEEE, Hang Li[©], Xuanhong Cheng, and James C. M. Hwang, Life Fellow, IEEE

Abstract-For the first time, the impedance spectrum of a live Jurkat T-lymphocytes human cell was characterized in a single sweep, spanning six decades of frequency from 9 kHz to 9 GHz. The ultra-wide bandwidth bridged the traditional impedance spectroscopy at kilohertz-megahertz frequencies with the recently developed microwave dielectric spectroscopy, which can probe the cell interior without being hindered by the cell membrane. Based on the measured scattering parameters and a simple cell model, an equivalent circuit of four nondispersive elements, including membrane resistance, membrane capacitance, cytoplasm resistance, and cytoplasm capacitance, was extracted and found sufficient to explain the so-called β relaxation over the frequencies measured. These extracted cell parameters are in general agreement with the literature but are believed to be more accurate, giving the relatively small standard deviations, the configuration with a cell in intimate contact with the measurement electrodes, and the ultra-wide bandwidth of the measurement.

Index Terms—Biological cells, biosensors, dielectric measurement, impedance measurement, microwave measurement, ultra-wideband (UWB) technology.

I. INTRODUCTION

OMPARED to conventional biochemical or optical techniques, electrical characterization of live biological cells can be fast, compact, and label-free as has been practiced for almost a century [1]. The technique is usually performed at kilohertz-megahertz frequencies and referred to as impedance spectroscopy [2] or dielectric spectroscopy [3].

In terms of impedance spectroscopy, a cell can be regarded as a complex impedance

$$Z = R + 1/j\omega C \tag{1}$$

Manuscript received December 7, 2017; revised June 14, 2018; accepted June 21, 2018. Date of publication July 10, 2018; date of current version August 6, 2018. This work was supported in part by the U.S. Department of Defense, Army Research Office under Contract W911NF-14-1-0665 and in part by the U.S. Air Force Office of Scientific Research under Grant FA9550-16-1-0475. This paper is an expanded version from the IEEE MTT-S International Microwave Workshop Series on Advanced Materials and Processes (IMWS-AMP 2017), Pavia, Italy, September 20–22, 2017. (Corresponding author: Xiao Ma.)

X. Ma, X. Du, and J. C. M. Hwang are with the Department of Electrical and Computer Engineering, Lehigh University, Bethlehem, PA 18015 USA (e-mail: xim214@lehigh.edu).

H. Li and X. Cheng are with the Department of Bioengineering and the Department of Materials Sciences and Engineering, Lehigh University, Bethlehem, PA 18015 USA.

Color versions of one or more of the figures in this paper are available online at http://ieeexplore.ieee.org.

Digital Object Identifier 10.1109/TMTT.2018.2851251

where R and C are often attributed to the cytoplasm and membrane, respectively, and $\omega = 2\pi f$ is the angular frequency proportional to the frequency f of the electrical signal. However, at kilohertz-megahertz frequenceies, the signal can barely penetrate through the membrane, and the measured resistance may be dominated by the membrane resistance R_M instead of the cytoplasm resistance R_C . In addition, the so-called "cytoplasm" resistance and capacitance are actually intracellular resistance and capacitance, with the effects of cytoplasm, nucleus, and other organelles lumped together.

In terms of dielectric spectroscopy, a cell can be regarded as a homogenous dielectric particle having a complex permittivity

$$\varepsilon = k\varepsilon_0 - j\sigma/\omega \tag{2}$$

where k is the dielectric constant, ε_0 is the vacuum permittivity, and σ is the conductivity. Again, at kilohertz—megahertz frequencies, the signal can barely penetrate through the membrane, and the measured dielectric constant may be dominated by that of the membrane k_M instead of that of the cytoplasm k_C .

Equations (1) and (2) are theoretically equivalent but relating them is not trivial. It involves many assumptions for the cell shape (spherical or not), the cell size dc, and the membrane thickness d_M . Often the electric field is simply assumed to be uniform and unperturbed by the cell. The relationship is even more complicated when cell suspensions are sampled, so that a mixture model such as the Maxwell-Wagner model [4] must be used to de-embed cell properties from that of the solution. The situation is further complicated by the polarization layers formed next to the electrodes due to ion movement in response to the signal at low frequencies [5]. To overcome the above-mentioned challenges, this paper focuses on single-cell ultra-wideband (UWB) impedance spectroscopy with a simple model and a minimum number of assumptions. Specifically, it focuses on impedance spectroscopy instead of dielectric spectroscopy, because the former can be more directly measured with fewer assumptions, especially in single-cell measurements.

When $f\gg 1$ MHz, ions are too slow to respond and the signal can penetrate through the cell membrane to sample its interior. In this case, a cell can be highly dispersive with different relaxation frequencies such as ω_{α} , ω_{β} , and ω_{γ} hypothesized more than 60 years ago [6] and is illustrated schematically in Fig. 1. As the result, frequency dependence

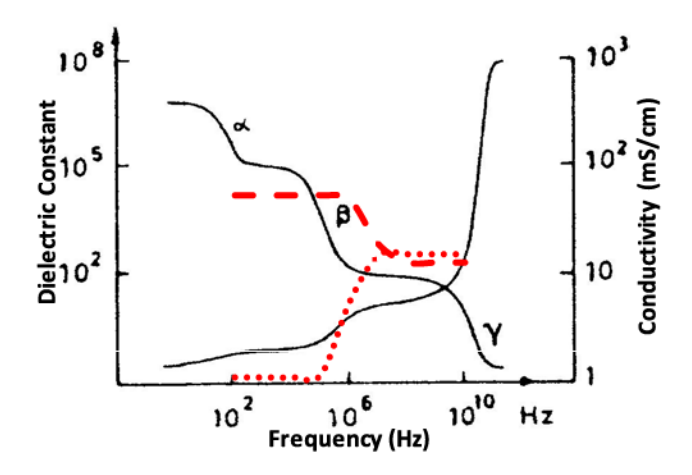


Fig. 1. Hypothesized [6] versus estimated dielectric constant (dashed curve) and conductivity (dotted curve) of a biological cell. The estimates are based on an equivalent circuit of four nondispersive elements: membrane resistance, membrane capacitance, cytoplasm resistance, and cytoplasm capacitance.

is often added to (1) and (2) so that

$$Z(\omega) = R(\omega) + 1/j\omega C(\omega)$$
 (3)

and

$$\varepsilon = \frac{\Delta \varepsilon_{\alpha}}{1 + j \omega / \omega_{\alpha}} + \frac{\Delta \varepsilon_{\beta}}{1 + j \omega / \omega_{\beta}} + \frac{\Delta \varepsilon_{\gamma}}{1 + j \omega / \omega_{\gamma}} \dots + \varepsilon_{\infty}$$

where $\Delta \varepsilon_{\alpha}$, $\Delta \varepsilon_{\beta}$, and $\Delta \varepsilon_{\gamma}$ represent the step heights across different relaxation frequencies and ε_{∞} represents the high-frequency limit. The physical meaning of frequency-dependent resistance and capacitance in (3) is questionable. Although (4) follows the well-known Debye formula, most materials are not dispersive below 100 MHz [7].

In [8], impedance spectroscopy was advanced to the single-cell level up to 40 GHz, so that not only the signal could readily penetrate through the cell membrane, but also the complications due to mixture modeling and electrode polarization could be avoided. Although a very attractive development, the lower frequency was limited by the typical vector network analyzer (VNA) to approximately 100 MHz, which had the opposite effect of making it difficult to extract membrane properties. It also made it difficult to relate the recent results obtained at microwave frequencies with the earlier results obtained at kilohertz—megahertz frequencies.

In [9], we first used a UWB VNA to characterize cells from 9 kHz to 9 GHz, which allowed us not only to avoid the limitations of using only kilohertz-megahertz frequencies or gigahertz frequencies, but also to relate the present result with the rich literature. In addition, we hypothesized that the dispersion of a cell did not necessarily originate from the dispersion of its individual compartments. Rather, the dispersion of a cell could be due to the heterogeneous combination of nondispersive compartments. Specifically, we were able to simulate the β relaxation of [6] from 1 kHz to 10 GHz by using an equivalent circuit of three nondispersive elements C_M , R_C , and C_C , where C_M and C_C are the capacitances of membrane

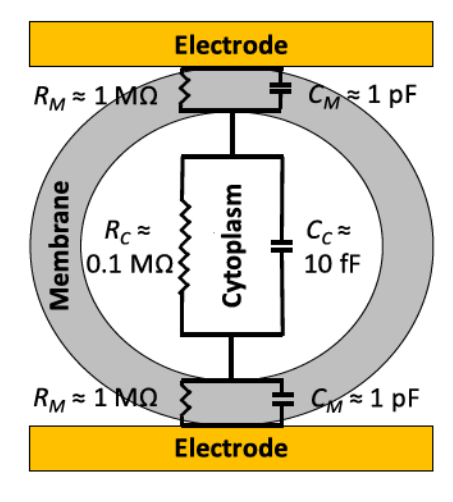


Fig. 2. Simple single-shell (double-layer) model of a cell with four equivalent-circuit elements comprising membrane resistance R_M , membrane capacitance C_M , cytoplasm resistance R_C , and cytoplasm capacitance C_C .

and cytoplasm, respectively. This paper expands the equivalent circuit to include four elements: R_M , C_M , R_C , and C_C . It also describes the theoretical analysis, experimental validation, and literature comparison in detail.

II. MODELING AND ANALYSIS

A. Equivalent-Circuit Model of a Cell

Fig. 2 illustrates a simple cell model comprising a spherical membrane enclosing homogeneous cytoplasm [10], thus lumping the contribution from the nucleus and other organelles together with that of cytoplasm as mentioned earlier. Typically, the properties of the membrane and cytoplasm of a mammalian cell are such that $d_M \approx 10$ nm [11], $dc \approx 10$ μ m, $k_M \approx 10$ [7], $k_C \approx 100$ [12], $\sigma_M \approx 10^{-4}$ S/m [13], and $\sigma_C \approx 1$ S/m [14]. For Jurkat T-lymphocytes human cells used in the present experiment, we confirmed by a Coulter counter that their median diameter was 9.7 μ m.

Presently, the simple cell model without the complication of the solution can be used because of the following.

- 1) The electrodes are in intimate contact with the cell as illustrated in Fig. 2, because the electrode spacing at 10 μ m is comparable to the cell size.
- Electrode polarization is further reduced because cells are resuspended in isotonic sucrose solution, which has low conductivity yet is sufficient to keep cells alive for hours [15].
- 3) Most of the electric field goes through the cell because the cytoplasm is more conductive than the solution, except at low frequencies when the field is blocked by the cell membrane.

The field distribution has been confirmed by 3-D finite-element electromagnetic simulation [16].

The simple cell model can be used to relate (3) and (4). For the order-of-magnitude estimate, the cell can be further simplified as a 10 μ m \times 10 μ m \times 10 μ m cube that is covered by 10-nm-thick membranes on both the top and bottom surfaces.

In this case, the cell can be represented by an equivalent circuit shown in Fig. 2 with four nondispersive elements

$$R_M = d_M / \sigma_M d_C^2 \approx 1 \text{ M}\Omega \tag{5}$$

$$C_M = k_M \varepsilon_0 d_C^2 / d_M \approx 1 \text{ pF}$$
 (6)

$$R_C = 1/\sigma_C d_C \approx 0.1 \text{ M}\Omega \tag{7}$$

and

$$C_C = k_C \varepsilon_0 d_C \approx 10 \text{ fF.}$$
 (8)

B. Modeled Impedance Spectrum

For impedance spectroscopy, the cell impedance according to the equivalent circuit of Fig. 2 is

$$Z = \frac{2R_M}{1 + (\omega/\omega_M)^2} + \frac{R_C}{1 + (\omega/\omega_C)^2} - j\omega \left[\frac{2R_M/\omega_M}{1 + (\omega/\omega_M)^2} + \frac{R_C/\omega_C}{1 + (\omega/\omega_C)^2} \right]$$
(9)

where $\omega_M = 1/R_M C_M \approx 1$ MHz and $\omega_C = 1/R_C C_C \approx 1$ GHz. Since $\omega_M \ll \omega_C$, (9) can be evaluated at three frequency ranges of $\omega \ll \omega_M$, $\omega_M \ll \omega \ll \omega_C$, and $\omega \gg \omega_C$, respectively.

If $\omega \ll \omega_M$

$$R = 2R_M + R_C \approx 2R_M \tag{10}$$

and

$$C = \frac{1}{\omega^2 (2R_M/\omega_M + R_C/\omega_C)} \approx \frac{C_M}{2(\omega/\omega_M)^2}$$
 (11)

where the approximation is justified by $R_M \gg R_C$ and $\omega_C \gg \omega_M$. As expected, at the low-frequency limit, the cell impedance is mainly due to membrane properties instead of cytoplasm properties. Specifically, for low-frequency impedance spectroscopy, (10) indicates that the resistance measured should not be mistaken as the cytoplasm resistance, and (11) indicates that the increasing capacitance with decreasing frequency should not be mistaken as an increasing dielectric constant of either the membrane or the cytoplasm.

If $\omega \gg \omega_C$

$$R \approx \frac{2R_M}{(\omega/\omega_M)^2} + \frac{R_C}{(\omega/\omega_C)^2} \approx \frac{R_C}{(\omega/\omega_C)^2}$$
 (12)

and

$$C \approx \frac{1}{2/C_M + 1/C_C} \approx C_C \tag{13}$$

where the approximation is justified by $C_M \gg C_C$ and $\omega_C \gg \omega_M$. As expected, at the high-frequency limit, the cell impedance is mainly due to cytoplasm properties instead of membrane properties. However, (12) indicates that the decreasing resistance with increasing frequency should not be mistaken as increasing cytoplasm conductivity, and (13) indicates that the constant capacitance implies a nondispersive cytoplasm dielectric constant.

If $\omega_M \ll \omega \ll \omega_C$

$$R \approx \frac{2R_M}{(\omega/\omega_M)^2} + R_C \tag{14}$$

and

$$C \approx \frac{1}{2/C_M + (\omega/\omega_C)^2/C_C}.$$
 (15)

As expected, (14) and (15) indicate that, whereas the low-frequency cell impedance is mainly due to membrane properties, in the intermediate frequency range, it is increasingly influenced by cytoplasm properties R_C and C_C through the weighing factors $(\omega/\omega_M)^2$ and $(\omega/\omega_C)^2$, respectively. Furthermore, the measured R and C dispersions may be characterized by two different frequencies, ω_M and ω_C , respectively, instead of a single β relaxation frequency.

C. Modeled Dielectric Spectrum

For dielectric spectroscopy, the cell admittance according to the equivalent circuit of Fig. 2 is

$$Y = \frac{(G_M + j\omega C_M)(G_C + j\omega C_C)/2}{(G_M + j\omega C_M)/2 + (G_C + j\omega C_C)}$$

$$\approx \frac{[2G_M + (\omega/\omega_0)^2 G_C] + j\omega[2C_M + (\omega/\omega_0)^2 C_C]}{4 + (\omega/\omega_0)^2}$$
(16)

where $G_M = 1/R_M$, $G_C = 1/R_C$, and $\omega_0 = 1/R_C C_M \approx 10$ MHz ($f_0 \approx 1$ MHz). The approximation is justified by $R_M \gg R_C$ and $C_M \gg C_C$. As expected, at the frequency limits $\omega^2 \ll 2\omega_0^2 R_C/R_M$ and $\omega^2 \gg 2\omega_0^2 C_M/C_C$, (16) approaches $(G_M + j\omega C_M)/2$ and $G_C + j\omega C_C$, which reflects membrane and cytoplasm properties, respectively.

From (2),

$$Y = (\sigma + j\omega k\varepsilon_0) d_C \tag{17}$$

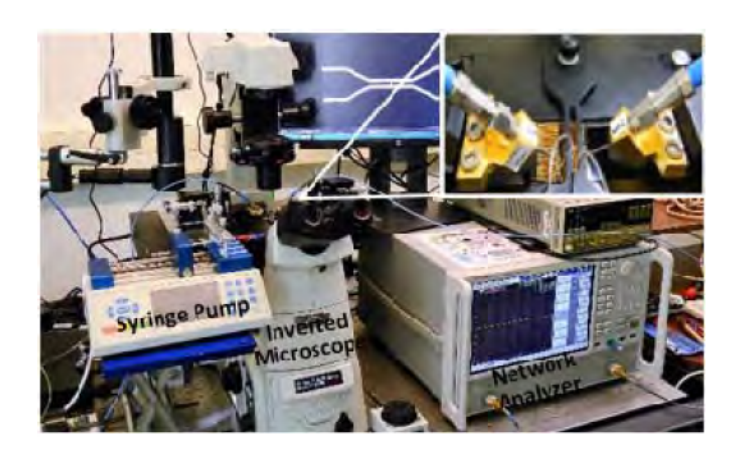
Equating (16) and (17),

$$\sigma \approx \frac{2G_M + (\omega/\omega_0)^2 G_C}{d_C [4 + (\omega/\omega_0)^2]} \tag{18}$$

and

$$k \approx \frac{2C_M + (\omega/\omega_0)^2 C_C}{\varepsilon_0 d_C [4 + (\omega/\omega_0)^2]}$$
 (19)

Using the order-of-magnitude estimates of dc, R_M , C_M , R_C , and C_C in (5)–(8), k and σ were calculated and found in qualitative agreement with that hypothesized by Schwan [6] and replicated in Fig. 1. It shows that the β relaxation can be captured by an equivalent circuit of four nondispersive elements R_M , C_M , R_C , and C_C . The analysis also shows that the β relaxation frequency around 1 MHz reflects the $R_C C_M$ time constant; the nearly constant values of k and σ below the β relaxation reflect C_M and R_M , respectively; the nearly constant values above the β relaxation reflect C_C and R_C , respectively. Although an equivalent circuit does not necessarily reflect the underlying physical mechanism, the above analysis shows that dispersive cell characteristics do not necessarily imply dispersive cell compartments and may originate from the heterogeneous combination of nondispersive compartments. Physically, the β relaxation is associated with membrane polarization without a sharply defined resonance frequency [6], and it manifests as an $R_C C_M$ resonance in the present measurement. However, in other measurement setups,



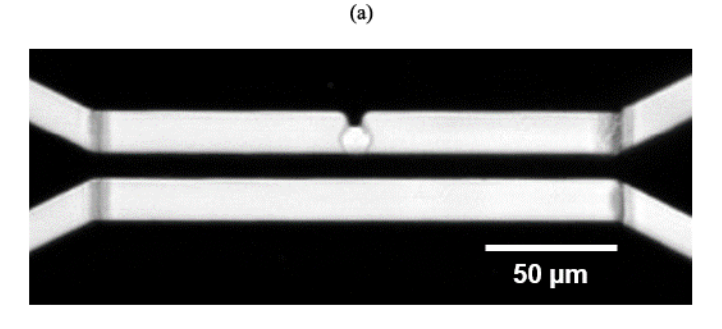


Fig. 3. (a) Photograph of the experimental setup for testing a CPW with a homemade probe station on an inverted fluorescence microscope. (b) Transmission micrographs of a Jurkat cell trapped near the middle of the CPW in the shunt configuration. Dark horizontal bands reflect metal electrodes, whereas dark vertical lines delineate microfluidic channel walls.

(b)

the series resistance may be dominated by parasitics, resulting in apparently different β relaxation frequencies.

III. EXPERIMENTAL SETUP AND MEASUREMENT PROTOCOL

Fig. 3(a) shows that the present setup for UWB electrical cell characterization comprises a homemade microwave probe station, on the top of a Nikon Eclipse Ti-E inverted fluorescence microscope equipped with a three-color video camera capable of 100 frames/s for simultaneous electrical measurement and video recording. The probe station is the device under test (DUT) connected through a pair of Cascade Microtech ACP40 GSG probes to a Keysight Technologies E5080A VNA for two-port measurement of scattering (S) parameters from 9 kHz to 9 GHz in a single sweep. The S parameters measured on the VNA were de-embedded to the probe tips using the short, open, load, and through standards of a Cascade Microtech 101-190 impedance-standard calibration substrate. The DUT is also connected to a microfluidic channel with its flow rate of cell suspension controlled at approximately 0.1 μ L/min by a syringe pump.

The DUT comprises a gold CPW, approximately 1 cm long and 0.5 μ m thick, on the top of a 0.5-mm-thick quartz substrate. A microfluidic channel intersects the CPW at a right angle, which is formed by 20- μ m-thick SU8 walls and a 5-mm-thick polydimethylsiloxane cover. With SU8 being a negative photoresist, the walls are lithographically defined

TABLE I

EQUIVALENT CIRCUIT PARAMETERS OF THE CPW
WITH AND WITHOUT A JURKAT CELL

Section	Parameter	Cell	Sucrose	Air	
Microfluidic Channel	Membrane Resistance R_M (M Ω)	1.5 ± 0.3			
	Membrane Capacitance $C_M(pF)$	1.5 ± 0.3 6.7		2.0	
	Cytoplasm Resistance R_C (M Ω)	0.4 ± 0.1	0.7	2.0	
	Cytoplasm Capacitance $C_C(fF)$	6.4 ± 0.1			
	Ground Capacitance C_G (fF)	26	26	3	
CPW under SU8	Characteristic Impedance $Z_{SU8}(\Omega)$	55			
	Electric Length @ 1 GHz θ_{SU8} (°)	1.4			
CPW under Air	Characteristic Impedance $Z_0(\Omega)$	43			
	Electric Length @ 1 GHz θ_0 (°)	3.8			
	$\operatorname{Loss} R_0\left(\Omega\right)$	$10^{-9} f (GHz) + 5$			

to be 2.4 mm wide and 200 μ m apart, leaving in between a microfluidic channel of 200 μ m wide and 20 μ m thick. Similarly, the width of the CPW center electrode is precisely tapered from 120 μ m outside the channel to 10 μ m inside the channel, while maintaining a constant spacing of 16 μ m from the ground electrodes both inside and outside the channel. Fig. 3(b) shows that to trap a Jurkat cell in the shunt configuration, the middle of the CPW has a 6- μ m protrusion in one of the ground electrodes.

To validate the equivalent-circuit model described in Section II, live Jurkat cells were used due to their relatively large diameter, simple structure, and nonadherent nature. The cells were cultured under 5% CO₂ at 37 °C in a media based on Sigma-Aldrich RPMI 1640 with 10% fetal bovine serum, 100 unit/mL penicillin, and 100 μ g/mL streptomycin. The cells were then washed with 8.5% sucrose plus 0.3% dextrose and twice resuspended to a concentration of approximately 3×10^6 cell/mL before injection through the microfluidic channel. In a separate experiment with Trypan Blue dye, more than half the cells were found alive after 10 h [15]. Trypan Blue was never used on cells subjected to electrical characterization, so that they remain label-free.

Different from our previous multicell characterization experiments [15], the present UWB VNA was used not only for cell characterization, but also to trap a single cell by supplying the DEP signal at 10 MHz and 3 dBm [17]. With a cell trapped in the gap of the CPW and visually confirmed through the microscope and video recorded as shown in Fig. 3, the syringe pump was paused and the VNA was switched from the fixed-frequency mode to the sweep-frequency mode while the power was decreased from 3 to -18 dBm for cell characterization. With rapidly successive S parameters measured with and without a cell trapped, the changes in the S parameters were calculated and used to extract cell characteristics as described in Section IV. Such a differential measurement allowed the small difference with and without a cell to be reliably extracted.

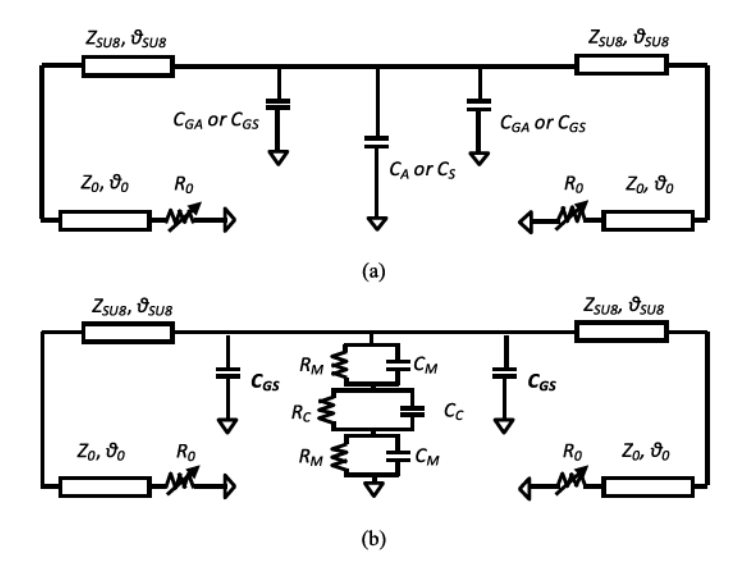


Fig. 4. (a) Equivalent circuit of a CPW comprising distributed sections under air $(Z_0, \theta_0, \text{ and } R_0)$ or SU8 $(Z_{SU8} \text{ and } \theta_{SU8})$ and a lumped section under air $(C_{GA} \text{ and } C_A)$ or sucrose solution (C_{GS}, C_S) . Resistors R_0 represent the frequency-dependent loss of the entire CPW. (b) Equivalent circuit with a cell trapped and C_S replaced by a parallel RC circuit.

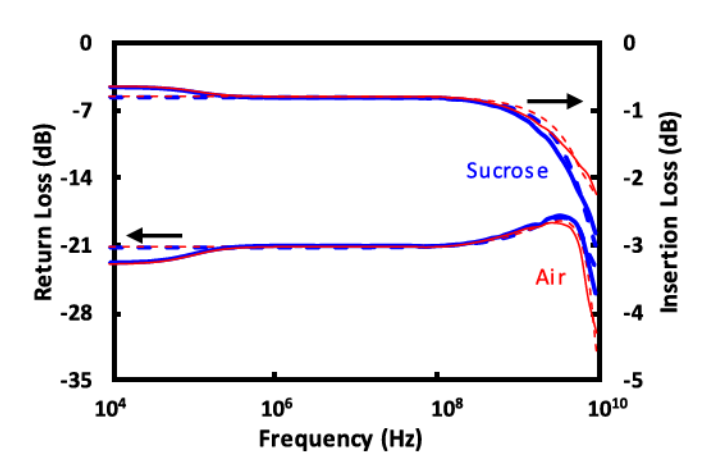
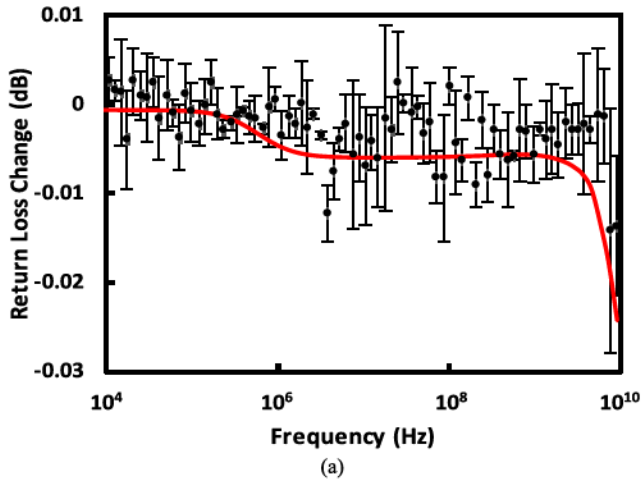


Fig. 5. Measured (solid curve) versus simulated (dashed curve) magnitudes of S_{11} and S_{21} with the microfluidic channel filled with air (red curve) and sucrose solution (blue curve), respectively.

IV. EXPERIMENTAL RESULTS AND DISCUSSION

To extract cell characteristics from the S parameters measured on the VNA and de-embedded to the probe tips, the equivalent circuit of Fig. 2 was expanded to include the CPW with a cell trapped, as shown in Fig. 4. The trapped cell was represented by the equivalent circuit of R_M , C_M , R_C , and C_C . Otherwise, the gap between the electrodes was simply represented by a shunt capacitance C_A or C_S associated with the air or sucrose solution, respectively. The short sections of the CPW inside the microfluidic channel were represented by shunt capacitance C_{GA} or C_{GS} , depending on whether the channel was empty or filled. Outside the channel, the CPW sections under SU8 and air were represented by distributed transmission lines with characteristic impedances Z_{SU8} and Z_0 , respectively, and electrical lengths θ_{SU8} and θ_0 , respectively. The above model parameters were extracted by the optimization module of Keysight's Advanced Design



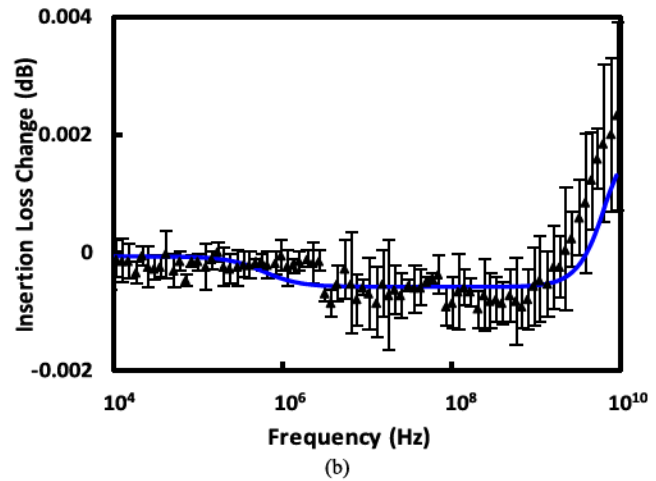


Fig. 6. Measured (symbol) versus simulated (curve) changes in (a) return loss and (b) insertion loss for the CPW with a live Jurkat cell trapped. Simulation performed with $R_M=1.5~\mathrm{M}\Omega$, $C_M=1.5~\mathrm{pF}$, $R_C=0.4~\mathrm{M}\Omega$, and $C_C=6.4~\mathrm{fF}$.

System with initial values estimated by Ansys HFSS simulation. The parameters are overdetermined and uncorrelated.

The loss of the entire CPW was captured in a frequencydependent resistance R_0 . Table I lists the equivalent-circuit element values extracted from S parameters measured with the microfluidic channel empty or filled. Fig. 5 shows that the S parameters simulated with the values listed in Table I agree with that measured except near the low- and highfrequency limits. At the low-frequency limit, both the return and insertion losses are not properly captured by the loss term R_0 , probably due to the double-layer formation [5]. Since this deficiency does not materially affect the accuracy of the present differential measurement, linearly dispersive R_0 is used to keep the equivalent circuit simple. For the same reason, the equivalent circuit does not explicitly account for water dispersion at the high-frequency limit. Overall, the smooth and low-loss S parameters across the ultra-wide bandwidth attest to the present CPW design and calibration techniques.

The change in the S parameters with a cell trapped, on the order of 0.01 dB or smaller, is not discernable on the scale of Fig. 5 and, hence, must be plotted separately. Fig. 6 shows the comparison of the measured and simulated

TABLE II
ELECTRICAL CHARACTERISTICS OF A JURKAT CELL

Bandwidth (MHz)	$R_M(M\Omega)$	$C_M(pF)$	$R_C(M\Omega)$	C_C (fF)	Reference
0.01-100	_	1.1	0.13	6	[18]
0.01-100	3.6	1.4	0.15	6	[13]
0.01-100	60-100	0.73 - 1.4	0.1 - 0.3	10-14	[19]
ns pulses	20	0.76 - 1.0	0.5	_	[20]
0.01-10	2	1.2	0.3	6	[21]
0.001-100	_	0.7	0.2	10	[22]
0.009-9000	1.5 ± 0.3	1.5 ± 0.3	0.4 ± 0.1	6.4 ± 0.1	This Work

changes (with respect to $|S_{11}|$ and $|S_{21}|$ measured without a cell trapped) in return loss $|S_{11}|$ and insertion loss $|S_{21}|$ for a single cell trapped. The measurement was repeated on three different cells as indicated by the error bars. These changes were used to extract cell characteristics, so that $R_M = 1.5 \pm 0.3 \, \mathrm{M}\Omega$, $C_M = 1.5 \pm 0.3 \, \mathrm{pF}$, $R_C = 0.4 \pm 0.1 \, \mathrm{m}\Omega$, and $C_C = 6.4 \pm 0.1 \, \mathrm{pF}$, as listed in Table I. The error terms in R_M , C_M , R_C , and C_C were estimated by sensitivity analysis [23]. It can be seen in Fig. 6 that the measured and simulated changes are in general agreement.

Table II shows that the extracted R_M , C_M , R_C , and C_C values are in general consistent with not only the order-of-magnitude estimate of (5)–(8), but also the literature. As mentioned in Introduction section, the impedance of a cell is more directly measurable, whereas the dielectric constant and conductivity of a cell are inferred only after many assumptions for the cell size, cell shape, membrane thickness, etc. Therefore, to facilitate the comparison of Table II, the dielectric constant and conductivity from dielectric spectroscopy measurements were converted to resistance and capacitance using a simple cubic cell of $10^3 \ \mu \text{m}^3$ as in (5)–(8).

In fact, in many cases listed in Table II, instead of extracting from measured data, R_C and C_C were estimated from the dielectric constant and conductivity of physiological saline [7], then included in an underdetermined cell model. We believe that, with C_C being on the order of 10 fF, it can only be reliably extracted at microwave frequencies such as in the present case. Lastly, R_M appears to be more scattered, probably due to the solution effect at the low-frequency limit. By contrast, the solution effect is minimized presently by resuspending cells in the low-conductivity sucrose solution.

V. CONCLUSION

The impedance spectroscopy of live Jurkat cells was characterized in a single sweep, spanning six decades of frequency from 9 kHz to 9 GHz. The ultra-wide bandwidth overcame the limitations of characterizations at only kilohertz-megahertz frequencies or only microwave frequencies, and allowed both membrane and cytoplasm characteristics to be reliably extracted through the same measurement. An equivalent circuit of four nondispersive elements, R_M , C_M , R_C , and C_C , was found sufficient to fit the so-called β relaxation over the frequencies measured. Although an equivalent circuit does not necessarily reflect the underlying physical mechanism, the analysis showed that dispersive cell characteristics do not necessarily imply dispersive cell compartments and may originate from the heterogeneous cell structure. The extracted

equivalent-circuit parameters are in general agreement with the literature but are believed to be more accurate, giving the relatively small standard deviations, the test setup with a cell in intimate contact with the measurement electrodes, and the ultra-wide bandwidth of the measurement.

The present analysis showed the nearly constant cell characteristics below the β relaxation could be used to extract membrane parameters such as C_M and R_M , whereas the nearly constant cell characteristics above the β relaxation could be used to extract cytoplasm parameters such as C_C and R_C . In addition, the β relaxation frequency and sharpness could be used for consistency check or to separate nuclear characteristics from cytoplasm characteristics. By expanding the equivalent circuit further to account for electrode polarization [24], the α relaxation could be included to extract even more cell parameters. Similarly, by including water dispersion [25], the γ relaxation could be included. However, with even wider bandwidth, the setup design and calibration technique need to be further improved. For example, multistate single-connection calibration with liquids of known dielectric properties [26] could be used to de-embed the measured S parameters to the liquid interface instead of the probe tip.

REFERENCES

- H. Fricke, "The electric capacity of suspensions with special reference to blood," J. Gen. Physiol., vol. 9, no. 2, pp. 137–152, Nov. 1925.
- [2] V. F. Lvovich, Impedance Spectroscopy: Applications to Electrochemical and Dielectric Phenomena. New York, NY, USA: Wiley, 2012.
- [3] V. Raicu and Y. Feldman, Dielectric Relaxation in Biological Systems: Physical Principles, Methods, and Applications. Oxford, U.K.: Oxford, 2015.
- [4] K. W. Wagner, "Explanation of electric relaxation processes based on Maxwell's ideas," Arch. Elektrotech., vol. 9, pp. 371–387, Sep. 1914.
- [5] H. P. Schwan, "Electrode polarization impedance and measurements in biological materials," *Ann. New York Acad. Sci.*, vol. 148, no. 1, pp. 191–209, Feb. 1968.
- [6] H. P. Schwan, "Electrical properties of tissue and cell suspensions," Adv. Biol. Med. Phys., vol. 5, pp. 147–209, May 1956.
- [7] C. Merla, M. Liberti, F. Apollonio, and G. D'Inzeo, "Quantitative assessment of dielectric parameters for membrane lipid bi-layers from RF permittivity measurements," *Bioelectromagnetics*, vol. 30, no. 4, pp. 286–298, May 2009.
- [8] T. Chen, F. Artis, D. Dubuc, J.-J. Fournié, M. Poupot, and K. Grenier, "Microwave biosensor dedicated to the dielectric spectroscopy of a single alive biological cell in its culture medium," in *IEEE MTT-S Int. Microw. Symp. Dig.*, Jun. 2013, pp. 1–4.
- [9] X. Ma et al., "One resistor and two capacitors: An electrical engineer's simple view of a biological cell," in *IEEE MTT-S Int. Microw. Symp. Dig.*, Sep. 2017, pp. 1–3.
- [10] A. Irimajiri, T. Hanai, and A. Inouye, "A dielectric theory of 'multi-stratified shell' model with its application to a lymphoma cell," J. Theor. Biol., vol. 78, no. 2, pp. 251–269, May 1979.
- [11] R. A. Meyer, "Light scattering from biological cells: Dependence of backscatter radiation on membrane thickness and refractive index," *Appl. Opt.*, vol. 18, no. 5, pp. 585–588, Mar. 1979.
- [12] X. Ma et al., "Reproducible broadband measurement for cytoplasm capacitance of a biological cell," in *IEEE MTT-S Int. Microw. Symp. Dig.*, May 2016, pp. 1–4.
- [13] I. Ermolina, Y. Polevaya, Y. Feldman, B. Z. Ginzburg, and M. Schlesinger, "Study of normal and malignant white blood cells by time domain dielectric spectroscopy," *IEEE Trans. Dielectr. Electr. Insul.*, vol. 8, no. 2, pp. 253–261, Apr. 2001.
- [14] K. R. Foster and H. P. Schwan, "Dielectric properties of tissues and biological materials: A critical review," *Critical Rev. Biomed. Eng.*, vol. 17, no. 1, pp. 25–104, 1989.
- [15] Y. Ning et al., "Broadband electrical detection of individual biological cells," IEEE Trans. Microw. Theory Techn., vol. 62, no. 9, pp. 1905–1911, Sep. 2014.

- [16] H. Li et al., "Distributed effect in high-frequency electroporation of biological cells," *IEEE Trans. Microw. Theory Techn.*, vol. 65, no. 9, pp. 3503–3511, Sep. 2017.
- [17] X. Du et al., "Ultra-wideband characterization, dielectrophoresis, and electroporation of a live biological cell using the same vector network analyzer," in IEEE MTT-S Int. Microw. Symp. Dig., Jun. 2018, pp. 1–4.
- [18] F. F. Becker, X.-B. Wang, Y. Huang, R. Pethig, J. Vykoukal, and P. R. C. Gascoyne, "Separation of human breast cancer cells from blood by differential dielectric affinity," *Proc. Nat. Acad. Sci. USA*, vol. 92, no. 3, pp. 860–864, 1995.
- [19] M. Kiesel et al., "Swelling-activated pathways in human T-lymphocytes studied by cell volumetry and electrorotation," Biophys. J., vol. 90, no. 12, pp. 4720–4729, Feb. 2006.
- [20] A. L. Garner et al., "Ultrashort electric pulse induced changes in cellular dielectric properties," Biochem. Biophys. Res. Commun., vol. 362, no. 1, pp. 139–144, Oct. 2007.
- [21] A. C. Sabuncu, J. Zhuang, J. F. Kolb, and A. Beskok, "Microfluidic impedance spectroscopy as a tool for quantitative biology and biotechnology," *Biomicofluidics*, vol. 6, no. 3, p. 034103, Jun. 2012.
- [22] S.-I. Han, Y.-D. Joo, and K.-H. Han, "An electrorotation technique for measuring the dielectric properties of cells with simultaneous use of negative quadrupolar dielectrophoresis and electrorotation," *Analyst*, vol. 138, no. 5, pp. 1529–1537, Jan. 2013.
- [23] X. Ma et al., "Sensitivity analysis for ultra-wideband 2-port impedance spectroscopy of a biological cell," *IEEE J. Electromagn.*, RF, Microw. Med. Biol., to be published.
- [24] J. C. Booth, N. D. Orloff, J. Mateu, M. Janezic, M. Rinehart, and J. A. Beall, "Quantitative permittivity measurements of nanoliter liquid volumes in microfluidic channels to 40 GHz," *IEEE Trans. Instrum. Meas.*, vol. 59, no. 12, pp. 3279–3288, Dec. 2010.
- [25] W. J. Ellison, "Permittivity of pure water, at standard atmospheric pressure, over the frequency range 0–25 THz and the temperature range 0–100 °C," J. Phys. Chem. Reference Data, vol. 36, no. 1, pp. 1–18, Feb. 2007.
- [26] X. Ma et al., "A multistate single-connection calibration for microwave microfluidics," *IEEE Trans. Microw. Theory Techn.*, vol. 66, no. 2, pp. 1099–1107, Feb. 2018.



Xiao Ma (S'15) received the B.S. degree in physics from Peking University, Beijing, China, in 2014. He is currently pursuing the Ph.D. degree in electrical engineering at Lehigh University, Bethlehem, PA, USA.

In 2016, he joined NIST, Boulder, CO, USA, as a foreign Guest Researcher of measurements and modeling for microwave microfluidic devices. His current research interests include biosensor, microwave measurement, liquid calibration, 3-D electromagnetic simulation using finite-element methods, and microwave device characterization techniques.



Xiaotian Du (GS'17) received the B.S. degree in materials science from Fudan University, Shanghai, China, in 2016. He is currently pursuing the Ph.D. degree in electrical engineering at Lehigh University, Bethlehem, PA, USA.

In 2014, he joined the University of California at Berkeley, Berkeley, CA, USA, as an Exchange Student. Since 2015, he has been a Research Assistant of electrical engineering with Lehigh University. His current research interests include biosensors, microelectromechanical systems, and other microwave devices and circuits.



Hang Li received the B.S. degree in chemical engineering and technology from Xi'an Shiyou University, Xi'an, China, in 2009, and the Ph.D. degree in chemical and biomolecular engineering from The University of Akron, Akron, OH, USA, in 2015.

Since 2015, he has been a Post-Doctoral Research Associate with Lehigh University, Bethlehem, PA, USA. His current research interests include mammalian cell electroporation and cell/bacterial membrane dynamic detection by broadband sensing.



Xuanhong Cheng received the B.S. degree in biology from Wuhan University, Wuhan, China, in 1998, and the M.S. degree in electrical engineering and Ph.D. degree in bioengineering from the University of Washington, Seattle, WA, USA, in 2004.

She held post-doctoral training with the Department of Surgery, Massachusetts General Hospital, Boston, MA, USA. In 2008, she joined Lehigh University, Bethlehem, PA, USA, where she is currently an Associate Professor with the Bioengineering Program and with the Department of Materials Science

and Engineering. Her current research interests include the development of microfluidic devices for cell and pathogen analysis. In combination with nanomaterials and biosensors, these devices are expected to perform automated sample processing and sensitive analyte detection toward point-of-care uses.



James C. M. Hwang (M'81-SM'82-F'94-LF'15) received the B.S. degree in physics from National Taiwan University, Taipei, Taiwan, and the M.S. and Ph.D. degrees in materials science and engineering from Cornell University, Ithaca, NY, USA.

He was with IBM, AT&T, GE, and GAIN. He cofounded GAIN and QED; the latter became a public company (IQE). Since 1988, he has been a Professor of electrical engineering with Lehigh University, Bethlehem, PA, USA. His current research interests include microwave biosensing, scanning

microwave microscopy, and 2-D atomic-layer materials and devices.